A Vibrational Sum Frequency Spectroscopy Study of the Liquid−Gas Interface of Acetic Acid−Water Mixtures: 2. Orientation Analysis

Eric Tyrode

Department of Chemistry, Surface Chemistry, Royal Institute of Technology, Drottning Kristinas Väg 51, SE-100 44 Stockholm, and YKI, Institute for Surface Chemistry, Stockholm, Sweden

C. Magnus Johnson*

Division of Corrosion Science, Royal Institute of Technology, Drottning Kristinas Väg 51, SE-100 44 Stockholm, Sweden

Steve Baldelli

Department of Chemistry, University of Houston, Texas 77204

Christofer Leygraf

Division of Corrosion Science, Royal Institute of Technology, Drottning Kristinas Väg 51, SE-100 44 Stockholm, Sweden

Mark W. Rutland

Department of Chemistry, Surface Chemistry, Royal Institute of Technology, Drottning Kristinas Väg 51, SE-100 44 Stockholm, and YKI, Institute for Surface Chemistry, Stockholm, Sweden

Received: June 18, 2004; In Final Form: October 15, 2004

Vibrational sum frequency spectroscopy has been used to investigate the surface of aqueous acetic acid solutions. By studying the methyl and carbonyl vibrations with different polarization combinations, an orientation analysis of the acetic acid molecules has been performed in the concentration range 0−100%. The surface tension of acetic acid solutions was also measured in order to obtain the surface concentration. The orientation of the interfacial acetic acid molecules was found to remain essentially constant in an upright position with the methyl group directed toward the gas phase in the whole concentration range. The tilt angle (θ_{CH_3}) of the symmetry axis of the methyl group with respect to the surface normal was found to be lower than 15° when considering a δ distribution of angles or as narrow as $0 \pm 11°$ when assuming a Gaussian distribution. Further investigations showed that the C═O bond tilt ($\theta_{C=O}$) of the acetic acid hydrated monomer was constant and close to 55° in the concentration range where it was detected. Finally, the orientation information is discussed in terms of different species of acetic acid, where the formation of a surface layer of acetic acid cyclic dimers is proposed at high acid concentrations.

1. Introduction

This paper is an extension of the preceding paper in this issue, in which the interfacial behavior of different kinds of acetic acid aggregates and water was treated. Aqueous solutions of acetic acid have been extensively studied by IR[1,2] and Raman[3−7] spectroscopy. However, those studies have only been concerned with the bulk behavior, whereas in the preceding paper, the surface composition and structure have been investigated by vibrational sum frequency spectroscopy (VSFS). The major conclusions of that paper concern the tendency of acetic acid to be enriched in the surface region, the types of acetic acid aggregates (hydrated monomer, linear dimer, and cyclic dimer) present at the surface at various concentrations, and assignments of absorption bands. This paper will concentrate on determining the orientation of interfacial acetic acid molecules.

A detailed knowledge of the orientation of interfacial molecules is of importance for a range of surface phenomena such as lubrication, foaming, reaction catalysis, adhesion, and biomembrane functions.[8] The theory behind orientation analysis has been described in several papers[9−12] and has usually been applied to determinations of the orientation of terminal methyl groups of carbon chains, though studies on other molecules such as water,[13] acetonitrile,[14] and ammonia[15] have also been performed.

In this report, three vibrations of the acetic acid molecule have been used in order to determine the average orientation of the molecules residing at the liquid−gas interface: the symmetric methyl stretch, asymmetric methyl stretch, and the C═O stretching vibration. A comparison of the experimentally determined orientations of these groups, combined with the geometrical constraints imposed by the bonding scheme, has made it possible to narrow the uncertainty in the calculation of the orientation of the whole molecule at the surface. To further refine the analysis of the interface, studies of the structuring of water molecules have also been performed. The orientation of the interfacial water molecules has been determined by means of the free (non-hydrogen-bonded) OH bond, which protrudes out into the gas phase.

* Corresponding author. Fax: + 46 8 208284. E-mail: magnusj@kth.se.

10.1021/jp047337y CCC: $30.25
Published on Web 12/03/2004

2. Theory

The theory of sum frequency generation (SFG) has been described briefly in the preceding paper in this issue and more extensively in other sources.[16,17] What follows here is a short summary of the basic concepts of VSFS and a more detailed explanation of orientation studies of interfacial molecules.

VSFS is a nonlinear second-order vibrational laser spectroscopy technique with the advantage of only probing molecules with an average net orientation. Thereby, it enables studies of the very few molecules at interfaces, with no contribution from the centrosymmetric bulk medium, under the electric dipole approximation. The technique involves the combination of a fixed visible and a tuneable IR pulsed laser beam at the surface. These two beams interact with interfacial molecules, and a third beam with the sum frequency (SF) of the two incoming beams is generated. When the frequency of the IR beam approaches one of the resonant vibrations of the species present at the surface, the SF signal is resonantly enhanced, making this technique very suitable for surface vibrational spectroscopy.

Three coordinate systems are normally used to conveniently describe the SF process: the molecule, the surface, and the laboratory fixed system. The molecule system $\alpha\beta\gamma$ ($\alpha, \beta, \gamma = a, b, c$) is suitable for describing for example selection rules, molecular symmetry elements, vibrational and electronic resonance effects, polarizabilities, hyperpolarizabilities, and other molecular properties. The surface fixed system *ijk* ($i, j, k = x, y, z$) is associated with the characteristics of the interface, and the laboratory fixed system *IJK* ($I, J, K = X, Y, Z$) describes the tensor components directly in terms of the features observed in the SF spectrum, with the *XY* plane parallel to the surface and the *Z* axis parallel to the surface normal (all laser beams propagate in the *XZ* plane). In the case of an isotropic surface, as the one considered here, the last two coordinate systems coincide. The orientation of the molecule is given in terms of the Euler angles, χ, θ, and ϕ, which represent the rotation of the molecular axes (*abc*) with respect to laboratory fixed axes (*XYZ*). χ refers to the azimuthal angle which corresponds to the angle of rotation around the surface normal, θ to the tilt from the surface normal, and ϕ to the twisting, which is the angle between the *a* axis and the *cZ* plane.

The SFG intensity is proportional to the square of the second-order nonlinear susceptibilities, $\chi^{(2)}_{IJK}$, the intensities of the visible (I_{vis}) and infrared (I_{IR}) electric fields, and the square of the Fresnel factors. $\chi^{(2)}_{IJK}$ can be conveniently divided into two terms: one nonresonant and one resonant describing the vibrational interactions. By performing experiments with different polarization combinations of the laser beams, the relationships of the different $\chi^{(2)}_{IJK}$, when adjusted for the Fresnel factors and the electric fields, determine the orientation of the bond. The Fresnel factors depend on the optical configuration and the refractive indices, both of the interface and the bulk phases involved in SF process. The $\chi^{(2)}_{IJK}$ are proportional to the orientationally averaged hyperpolarizabilities $\langle\beta^{(2)}_{IJK}\rangle$, which describe the average orientation of the interfacial molecules. $\beta^{(2)}_{IJK}$ is in turn related to the hyperpolarizability in molecular coordinates ($\beta^{(2)}_{\alpha\beta\gamma}$) through a sixth-ranked tensor of direction cosines defined in terms of the Euler angles.[10] Finally, the $\beta^{(2)}_{\alpha\beta\gamma}$ can be expressed as the product of the Raman polarizability tensor component ($\alpha_{\alpha\beta}$) and the IR transition dipole moment (μ_γ), according to eq 1

$$\beta^{(2)}_{\alpha\beta\gamma} = \frac{\langle g|\alpha_{\alpha\beta}|v\rangle\langle v|\mu_\gamma|g\rangle}{\omega_n - \omega_{IR} - i\Gamma_n} \qquad (1)$$

where g is the ground state, v is an excited state, ω_{IR} is the frequency of the infrared laser beam, ω_n is a vibrational transition frequency, i is the imaginary unit, and Γ_n is the damping constant. The individual elements of the Raman tensor are normally difficult to obtain with enough accuracy. Nevertheless, when the Raman tensor has only two independent components, the experimentally accessible depolarization ratio can be used to determine their relative values.

For an isotropic liquid surface, there are four polarization combinations that give rise to a nonzero SF signal: ssp, sps, pss, and ppp, where the letters designate the polarization, whether parallel (p) or perpendicular (s) to the plane of incidence of the SF, visible, and IR, respectively. Each of the four polarization combinations probe different components of $\chi^{(2)}_{IJK}$. The first three (ssp, sps, and pss) each depend on a single component of the nonlinear susceptibility ($\chi^{(2)}_{YYZ}$, $\chi^{(2)}_{YZY}$, and $\chi^{(2)}_{ZYY}$, respectively). On the other hand, ppp probes an admixture of four components: $\chi^{(2)}_{ZZZ}$, $\chi^{(2)}_{ZXX}$, $\chi^{(2)}_{XZX}$, and $\chi^{(2)}_{XXZ}$. Because these experiments are performed far away from electronic transitions, the Raman tensor is symmetric, implying that the first two indices of $\chi^{(2)}$ can be exchanged without modifying the respective tensor elements (i.e., $\chi^{(2)}_{YZY} = \chi^{(2)}_{ZYY}$). Therefore, sps and pss spectra only differ by a constant, which is related to the Fresnel factors. Because the surface is isotropic, the following relations also hold: $\chi^{(2)}_{XZX} = \chi^{(2)}_{YZY}$, $\chi^{(2)}_{ZXX} = \chi^{(2)}_{ZYY}$. Altogether, three independent nonzero susceptibilities remain: $\chi^{(2)}_{YYZ}$, $\chi^{(2)}_{YZY}$, and $\chi^{(2)}_{ZZZ}$.

3. Experimental Methods

3.1. Vibrational Sum Frequency Spectroscopy (VSFS). What follows is a brief summary of the experimental setup. A detailed description is given in the preceding paper in this issue. A Nd:YAG laser (1064 nm, 20 Hz, 24 ps) from Ekspla is used to pump an OPG/OPA from LaserVision, generating both a visible (532 nm) and a tuneable IR output beam of 1.4−12 μm. Shorter wavelengths are produced by KTP and KTA crystals, whereas wavelengths longer than 5 μm require an additional $AgGaSe_2$ crystal. The bandwidth is 7−9 cm^{-1} for wavelengths shorter than 5 μm and <15 cm^{-1} for wavelengths greater than 5 μm. The visible beam is generated by a KTP doubling crystal. The optical setup is in a copropagating geometry with angles from the surface normal of 55° and 63° for the visible and IR beams, respectively. After passing through a monochromator, the SF beam is detected with a photomultiplier tube (PMT) and processed by an integrated boxcar and a Labview program.

The spectra were fitted by Lorentzian line shapes of the form shown in eq 2, employing the Origin software, using the χ^2 minimization routine with the instrumental weighting method, which accounted for the experimental scatter in the data.

$$I_{SFG}(\omega_{IR}) = \left|\chi^{(2)}_{NR} + \sum_n \frac{A_n}{\omega_n - \omega_{IR} - i\Gamma_n}\right|^2 \qquad (2)$$

where χ_{NR}, A_n, ω_{IR}, ω_n, and Γ_n refer to the nonresonant contribution to the SF signal, amplitude (oscillator strength), infrared light frequency, peak position, and damping constant of the *n*th resonant mode, respectively. VSF spectra are normally more complex than IR and Raman spectra. The asymmetry of most of the SF bands is due to interference, whether destructive or constructive, with adjacent vibrational modes and/or the nonresonant background. This is accounted for by the χ_{NR} term and the squared factor in eq 2.

3.2. Raman Spectroscopy. A BioRad FTS6000 with a Raman accessory, equipped with a setup for polarization

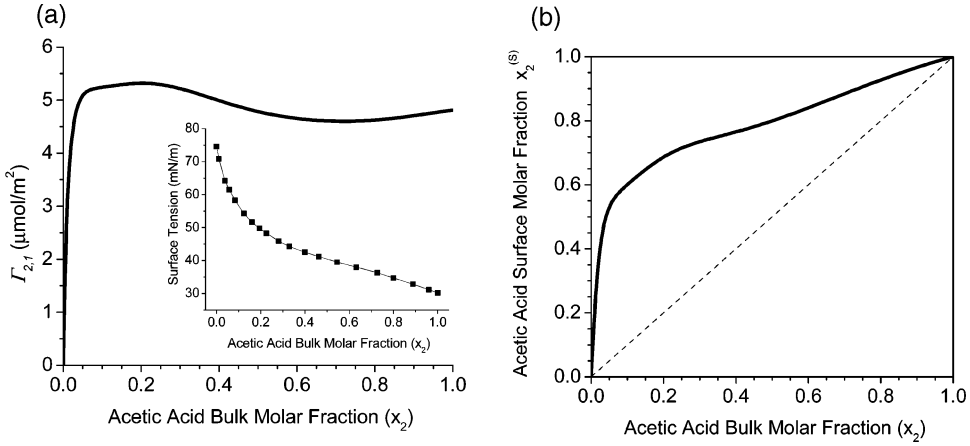

Figure 1. (a) Relative adsorption of acetic acid in aqueous solution. The inset shows the surface tension of water−acetic acid solutions at 4 °C. (b) The surface mole fraction of acetic acid as a function of the bulk mole fraction, calculated on the basis of the monolayer model.

measurements, was used to determine the depolarization ratios of normal modes of aqueous acetic acid solutions. Depolarization ratios were obtained after averaging over at least 2056 spectra with a resolution of 4 cm^{-1}, using a 180° scattering geometry. The spectra were fitted using both Lorentzian and Voigt profiles, which returned the same ratios. Though in principle simple, accurate measurements of the depolarization ratios are by no means trivial to obtain and must be performed with great care.[18]

3.3. Surface Tension. Surface tension was measured with a Krüss K12 tensiometer, employing the Wilhelmy plate method. The platinum plate was sand-blasted to ensure a zero contact angle at the three-phase contact line. The surface tension was calculated from the following expression:

$$F = 2\gamma(L_T + L_W) + L_T L_W \Delta\rho g h \qquad (3)$$

where F is the measured force, γ the surface tension of the liquid−vapor interface, L_T and L_W the thickness and the width of the plate, respectively, $\Delta\rho$ the density difference between the liquid and vapor phases, g the gravitational constant, and h the immersion depth of the plate in the liquid. All measurements were performed at 4.0 ± 0.2 °C.

4. Results and Discussion

4.1. Surface Concentration. The number of acetic acid molecules (N) present at the surface can be estimated from surface tension and liquid−vapor equilibrium data. The surface and bulk concentration can differ significantly, especially with surface-active molecules such as acetic acid in water. The driving force to the surface is the hydrophobic methyl group of the acid, which displaces water molecules and thus annihilates air−water surface area, representing a considerable free energy gain for the system that lowers the chemical potential of the acetic acid at the surface. The relative adsorption ($\Gamma_{2,1}$) can be related to the surface tension (γ) using the Gibbs equation:

$$-\left(\frac{\partial\gamma}{\partial\mu_2}\right) = -\frac{\left(\frac{\partial\gamma}{\partial x_2}\right)_{T,p}}{\left(\frac{\partial\mu_2}{\partial x_2}\right)_{T,p}} = -\frac{x_2}{RT}\left[\frac{\left(\frac{\partial\gamma}{\partial x_2}\right)_{T,p}}{1 + x_2\left(\frac{\partial \ln f}{\partial x_2}\right)}\right] = \Gamma_{2,1} = \Gamma_2 - \Gamma_1\frac{x_2}{x_1} \qquad (4)$$

where x_i refers to the bulk molar fraction of component i (1 → water, 2 → acetic acid), μ to the chemical potential ($\mu_2 = \mu^\circ_2 + RT \ln x_2 f$), f to the activity coefficients of acetic acid−water mixtures, R to the universal gas constant, and T to the temperature. The relative adsorption is independent of the position of the dividing surface, in contrast to the actual water (Γ_1) and acid (Γ_2) adsorptions. Surface tension was measured experimentally (see inset in Figure 1a), while the activity coefficients were obtained using the UNIFAC equations[19] which agreed with experimental data.[20] Because $\Gamma_{2,1}$ depends on the derivative of the activity coefficients, highly precise data should be used to avoid the introduction of uncertainties in the calculated surface excess. An alternative method based on light scattering[21] should allow the osmotic compressibility ($\partial\mu/\partial x$) of binary mixtures to be obtained directly, leading to greater accuracy in $\Gamma_{2,1}$. However, for the purpose of our analysis, the approach based on activity coefficients is considered to be sufficient. The relative adsorption is depicted in Figure 1a showing a positive value, which proves that the acetic acid is enriched at the surface with respect to the bulk in the whole concentration range.

To a first approximation, the surface concentration can be calculated on the basis of the monolayer model,[22−24] with the added assumption that the surface molecular areas of the acid (a_2) and water (a_1) are known and deemed to be concentration-independent. This last supposition will prove to be accurate in the light of the SF results to be discussed later, because the orientation of the acid molecules remains constant over the whole concentration range. The surface molar fraction of acetic acid (x_2^s), can be evaluated using eqs 5 and 6 in conjunction with eq 4.

$$N_{Av}(\Gamma_1 a_1 + \Gamma_2 a_2) = 1 \qquad (5)$$

$$x_2^s = \frac{\Gamma_2}{\Gamma_2 + \Gamma_1} \qquad (6)$$

where N_{Av} is Avogadro's number. The surface area per molecule for water and acid were taken to be 8 [24] and 24 Å^2 respectively, the latter being the area per molecule of compressed Langmuir−Blodgett films of long-chain fatty acids.[25] Figure 1b shows x_2^s versus x_2 which can be considered representative of the real system, bearing in mind the assumptions and approximations taken.

4.2. Sum Frequency Spectra. For ssp polarization in the region above 2680 cm^{-1}, six distinct peaks[26] were used to fit the spectra: the symmetric methyl stretch at ∼2946 cm^{-1}, the OH stretch of hydrogen-bonded acetic acid at ∼2975 cm^{-1}, two

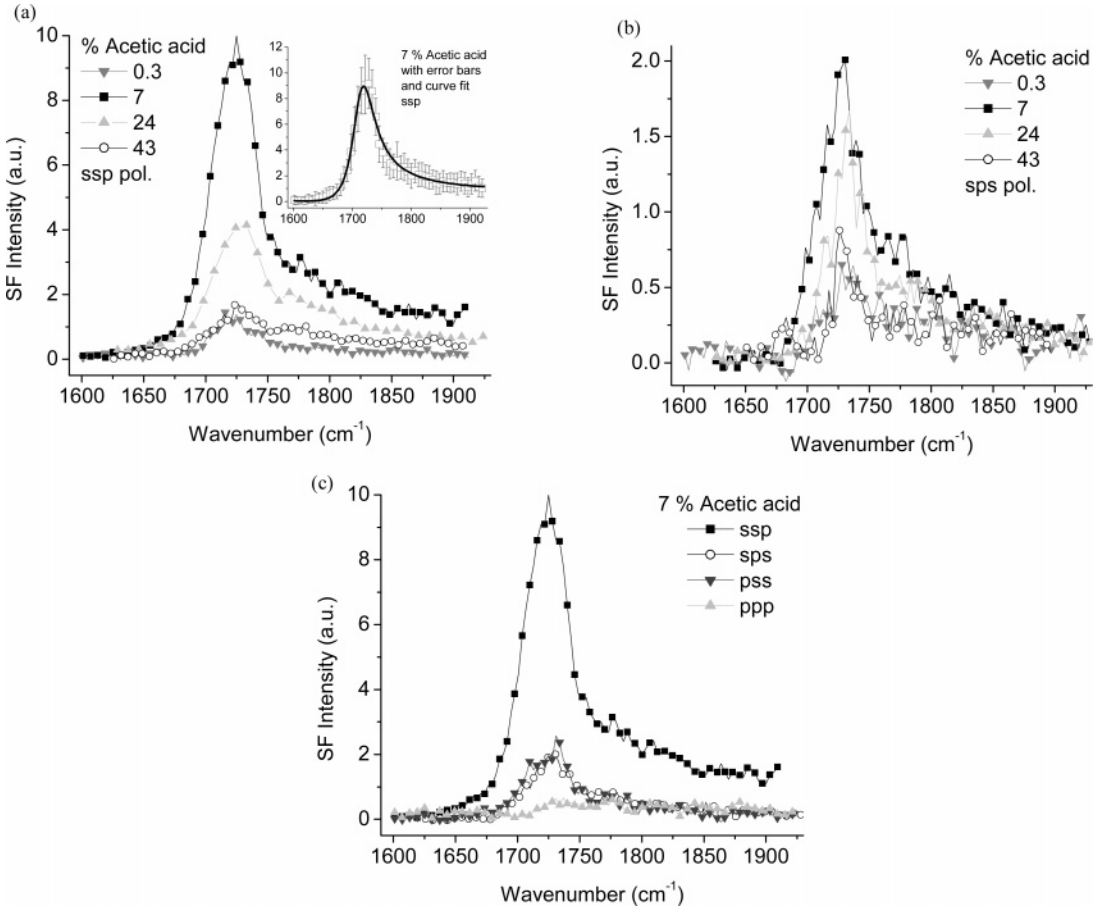

Figure 2. SFG spectra of the C═O stretching vibration at different bulk concentrations using the ssp (a) and sps (b) polarization combination. Inset in part a shows the error bars of the experimental data and fitting curve. (c) SFG spectra of ν(C═O) at 7% acid in four different polarization combinations: ssp, sps, pss, and ppp. In all figures, only every second point is shown for clarity. Lines shown are guides to the eye.

OH stretching peaks for hydrogen-bonded water at ∼3250 and ∼3420 cm^{-1}, the weakly/non-hydrogen-bonded OH stretch of water at ∼3620 cm^{-1}, and the free OH stretch of water at 3702 cm^{-1}. In the ppp spectra, the asymmetric methyl stretch at 2970 cm^{-1} was also included. All fitting parameters were allowed to vary. Finally, only one Lorentzian peak centered around 1720 cm^{-1} was used for the C═O range under all polarizations studied.

In all cases, the nonresonant background was constrained to be real, because for dielectric surfaces such as the one considered here, the imaginary part is expected to be zero, far away from electronic transitions.[27] In the inset in Figure 2a, and in Figure 5 for ssp and sps polarizations at 7% (all concentrations refer to bulk mole percent acetic acid, unless otherwise stated), the fitting curve and error bars are included, showing the fit quality and dispersion in the experimental data. The C−O stretch was not used in the orientation analysis because of its weak SF signal.

4.2.1. The C═O Stretching Range. Spectra of the C═O stretching vibration ν(C═O) were taken at four polarization combinations, ssp, sps, pss and ppp, of which the first three gave good signal-to-noise ratio in a broad concentration range. The ppp polarization only gave rise to well-defined peaks at a few concentrations. As expected, the spectra with pss polarization only differed from the sps spectra by a constant factor. Figure 2a and b show spectra of the C═O region of different concentrations for the ssp and sps polarizations, and Figure 2c shows all four polarizations for 7% acetic acid.

In all spectra shown, only one distinct peak is seen. There is a significant constructive interference with the nonresonant background at the high wavenumber side, which causes the tail to extend far away from the peak center. The fact that a single peak is observed leads to the interpretation that there is only one species of acetic acid giving rise to the SF signal at all concentrations. As described in detail in the preceding paper,[26] the peak at 1720 cm^{-1} is ascribed to the stretching vibration of the C═O group of a hydrated monomer (M_h). In Figure 2c, it can be seen that the amplitude of the C═O stretch in the ssp spectrum is highest, followed by the sps and pss spectra with almost equal intensities, and finally, the ppp spectrum with the lowest intensity. These four polarizations have been used to determine the tilt angle of the C═O bond ($\theta_{C=O}$) as will be discussed later. The amplitude of the C═O stretching vibration (based on the spectra in Figure 2) as a function of the concentration of acetic acid is shown for the ssp and sps polarizations in Figure 3a. The damping constant ($\Gamma_{C=O}$) and nonresonant contribution (χ_{NR}) obtained from the fitting were essentially constant (20 ± 2 cm^{-1} and −0.12 ± 0.05 au, respectively) along the concentration range where the C═O peak was detected.

It is observed that the ssp and sps data show the same characteristics: the amplitude increases between 0.3 and 7% acetic acid, followed by a decrease in amplitude at higher concentrations. The peak is not observed after 43% for both the ssp and sps polarizations.

The SF peak amplitude is dependent on the surface number density and the orientation of the molecules. The results in Figure 3a are a combined effect of both those parameters, and to distinguish the contribution from the orientation alone, the amplitudes have been normalized to the surface number density

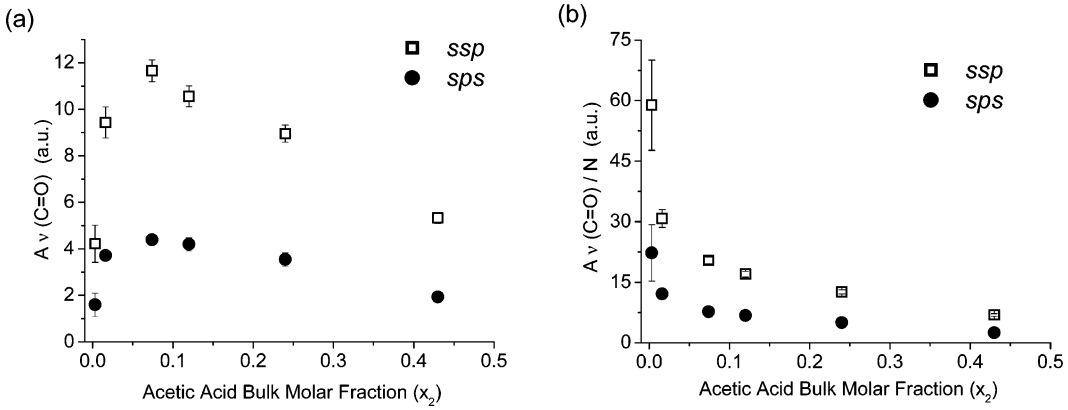

Figure 3. (a) Fitted amplitudes for the C═O stretching vibration (A_ν(C═O)) in the concentration range where it appears for ssp and sps polarization. (b) Normalized amplitudes for the C═O stretching vibration (A_ν(C═O)/N) in the ssp and sps polarization combinations.

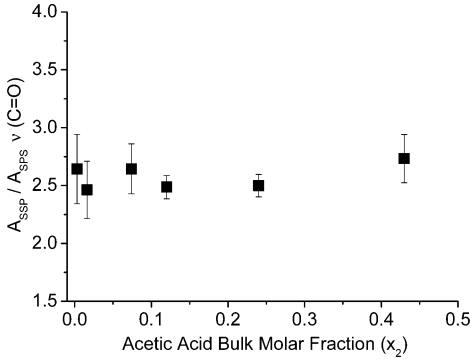

Figure 4. Ratio of the fitted amplitudes of the C═O stretching vibration (A_{ssp}/A_{sps}) in the concentration range where it appears.

N. The value of N, which is related to the surface molar concentration, is obtained from surface tension measurements as described already. Figure 3b thus displays the normalized amplitude (A_ν (C═O)/N), now only dependent upon the orientational characteristics of the molecules.

The normalized amplitudes of both the ssp and sps peaks initially decrease steeply with increasing concentration before leveling off at higher concentrations and disappearing at concentrations above 43% acetic acid. The fact that the normalized ssp signal decreases with increasing concentration would ordinarily be interpreted in terms of a larger tilt angle $\theta_{C=O}$ from the surface normal or a more random distribution of orientations of the C═O group. However, it will be revealed that none of these options are correct for this particular system. The data in Figure 4 show that the possibility of orientational changes can be discarded, as will be discussed in detail, while the second alternative of increased disorder is left to be refuted in a following section.

As can be observed in Figure 4, the A_{ssp}/A_{sps} ratio remains nearly constant and close to 2.6 for all concentrations measured, indicating that the orientation of the C═O bond is also practically invariant for concentrations up to 43% acetic acid, above which the C═O peak is below the detection limit for both the ssp and sps polarization. An essentially constant A_{ssp}/A_{sps} ratio rules out a change in the orientation of the C═O bond of the surface acetic acid molecules in the range where the peak is detected.

4.2.2. The CH/OH stretching range. SF spectra in the region extending from 2680 to 3900 cm^{-1} have been obtained for three polarizations: ssp, sps, and ppp. Figure 5 shows the spectra of 0, 0.3, and 7% acetic acid for the polarizations studied. The ssp spectra have already been treated in detail.[26] The spectra of pure water (top row) are in agreement with other published spectra,[28,29] though the relative intensities between the spectra obtained at different polarization combinations may differ depending on the optical configurations used because they are directly affected by the Fresnel factors, which depend on the angles of the incoming beams as discussed in the Theory section. In the ssp spectrum, there are two peaks from the OH stretch of hydrogen-bonded water molecules at approximately 3250 and 3420 cm^{-1} and one peak from the free OH at around 3702 cm^{-1}. The sps spectrum is difficult to interpret, but it is obvious that there are resonances above 3250 cm^{-1}. However, because of the lack of prominent features, it is not possible to use the sps spectrum of pure water for orientation analysis. The ppp spectrum of pure water shows a small peak in the hydrogen-bonded region with a maximum around 3500 cm^{-1} and a prominent peak at 3702 cm^{-1}, originating from the free OH.

Upon addition of small amounts of acetic acid, the spectra change drastically. It is interesting to note that it is only at 0.3% that the ssp spectrum shows the maximum number of peaks encountered from water and acetic acid in the whole concentration range studied. At all other concentrations, at least one peak is absent. In the ssp spectrum of 0.3% acetic acid, three new features appear, compared to the spectrum of pure water: the sharp peak at 2943 cm^{-1} ascribed to the symmetric methyl stretch $\nu_s(CH_3)$,[30] the broad band centered at ∼2975 cm^{-1}, which originates from the OH stretch of hydrogen-bonded acetic acid, and the small peak at approximately 3620 cm^{-1}, ascribed to weakly or non-hydrogen-bonded water.[26] At 0.3%, the intensities of the two hydrogen-bonded water peaks at ∼3250 and ∼3420 cm^{-1} and the free OH peak have significantly decreased in intensity compared to pure water. The sps spectrum of 0.3% also shows a clear peak at ∼3620 cm^{-1}, which, as for the ssp spectrum, is ascribed to weakly or non-hydrogen-bonded water. There is also an increasing intensity in going from 3400 cm^{-1} to lower wavenumbers in the sps spectrum, but no distinct peak can be discerned. However, the intensity is probably related to the OH stretch of hydrogen-bonded acetic acid, in accordance with the ssp spectrum. The ppp spectrum of 0.3% acetic acid also shows that the intensity of the free OH peak at 3702 cm^{-1} has decreased compared to the pure water spectrum. In the hydrogen-bonded region of water (3100−3500 cm^{-1}), there are no clear features. Slightly below 3000 cm^{-1}, a weak band associated with the methyl group appears for the first time and is discussed in detail in the following text.

The ssp spectrum of 7% acetic acid shows that the symmetric methyl stretch at 2943 cm^{-1} has grown significantly, as well as the OH stretch of hydrogen-bonded acetic acid at ∼2975

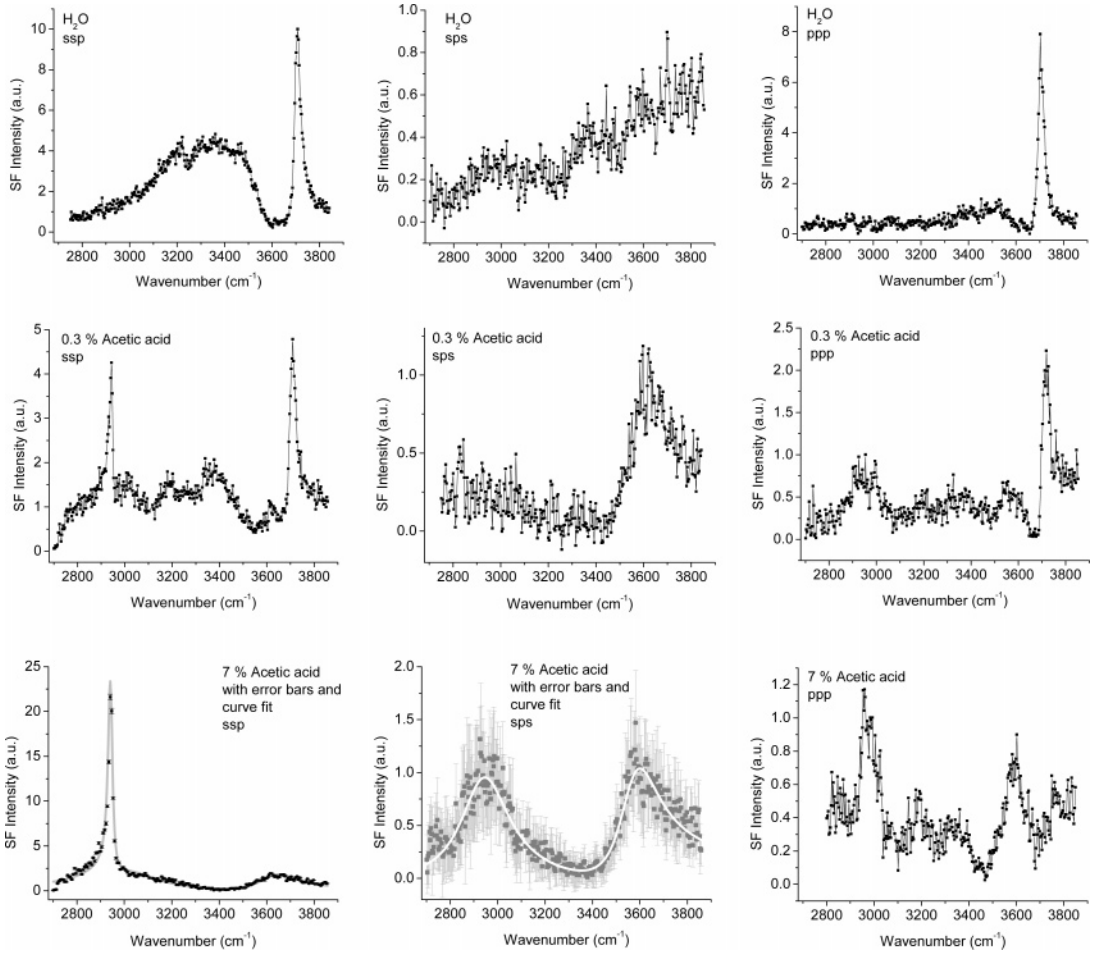

Figure 5. SF spectra of polarization combinations ssp, sps, and ppp for pure water, 0.3 and 7% acetic acid solutions. In the ssp and sps spectra for 7%, the fitting curves and experimental error bars are shown.

cm^{-1}. In contrast, the peaks originating from hydrogen-bonded water at ∼3250 and ∼3420 cm^{-1} and the free OH have vanished. However, the band of weakly or non-hydrogen-bonded water at ∼3620 cm^{-1} has increased in intensity. In the sps spectrum, the peak at ∼3620 cm^{-1} has grown slightly stronger compared to 0.3%. Another feature in the 7% sps spectrum is the broad peak at ∼2975 cm^{-1}, which in accordance with the 7% ssp spectrum is ascribed to the OH stretch of hydrogen-bonded acetic acid. In the 7% ppp spectrum, the peak assigned in the ssp and sps spectra to weakly or non-hydrogen-bonded water clearly appears at approximately 3620 cm^{-1}. A band centered at around 2970 cm^{-1}, already observed in the 0.3% ppp spectrum, is now also more clearly seen in the 7% ppp spectrum. This intensity is ascribed to the overlapping of two fundamental bands: the asymmetric methyl stretch $\nu_a(CH_3)$ at 2970 cm^{-1} and the broad OH stretching band of acetic acid at ∼2975 cm^{-1}. It is worth reminding that, because of the coherent nature of the SF beam, vibrational modes may constructively and/or destructively interfere with the nonresonant background, and in the case of overlapping bands, this interference can also involve the adjacent modes. As a result, the detected spectra can have a very asymmetric shape with some features convoluted and not directly observable. This is the case of the asymmetric methyl stretch $\nu_a(CH_3)$ and the broader OH stretching band of acetic acid in the ppp spectra. To clearly identify the asymmetric methyl stretch, spectra were collected of mixtures of 7% CH_3COOH in D_2O. Because of isotopic exchange, most of the acid in solution is found as CH_3COOD, removing the OH stretching band observed in the spectra of

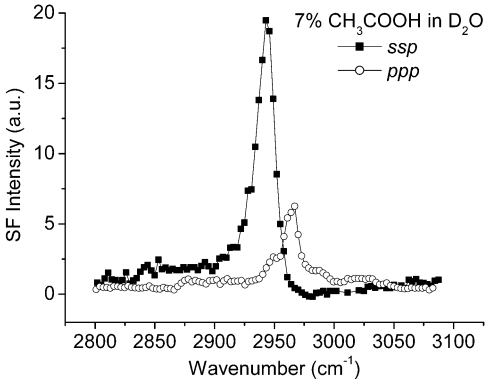

Figure 6. SF spectra of polarization combinations ssp and ppp for a 7% solution of CH_3COOH in D_2O. The asymmetric methyl stretch is clearly observed in the ppp spectrum at 2970 cm^{-1}.

fully protonated acid. In Figure 6, the ppp spectrum of such a mixture is shown (the ssp spectrum is also added for reference). The asymmetric methyl stretch $\nu_a(CH_3)$ is clearly identified as a narrow peak centered at 2970 cm^{-1}, which is approximately 30 cm^{-1} below the one observed in IR[31] and Raman spectra,[30] where it was reported only as a weak shoulder. Moreover, no evidence was found in the SF spectra for the other asymmetric methyl stretch $\nu_{s'}(CH_3)$ at 3051 cm^{-1}.[30]

The evolution of the ssp spectrum at higher concentrations has already been described in detail.[26] To summarize briefly, it can be said that the amplitudes of all peaks but the $\nu_s(CH_3)$ start to decrease at concentrations higher than 7% acetic acid

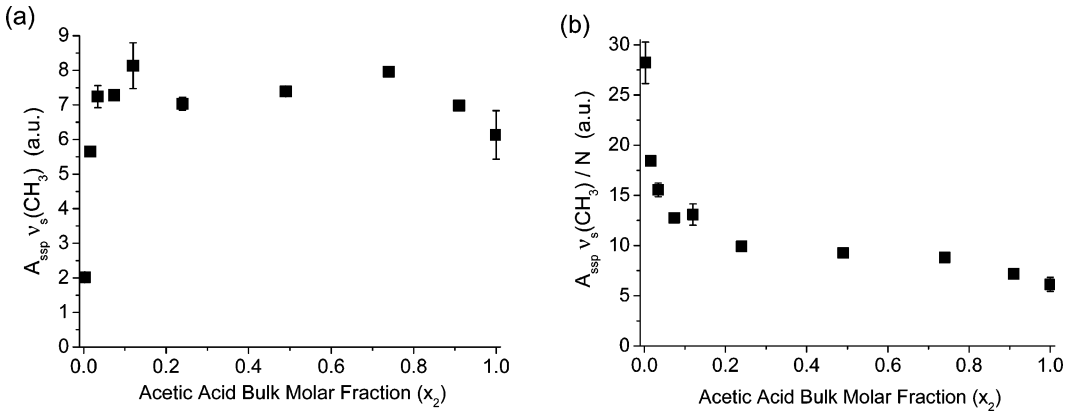

Figure 7. (a) Fitted amplitudes for the symmetric methyl stretching vibration (A_{SSP} $\nu_s(CH_3)$) in the whole concentration range for ssp polarized spectra. (b) Normalized amplitudes for $\nu_s(CH_3)$ (A_{SSP} $\nu_s(CH_3)/N$).

TABLE 1: Fitting Parameters for the Symmetric Methyl Stretch and Nonresonant Background in the CH/OH Stretching Region

concentration (mol %)	amplitude (au)	peak position (cm^{-1})	$\Gamma_{\nu_s(CH_3)}$ (cm^{-1})	χ_{NR} (au)
0.3	2.02 ± 0.15	2943 ± 1	8.5 ± 1.0	-0.04 ± 0.5
1.6	5.65 ± 0.10	2942 ± 2	8.5 ± 2.5	0.01 ± 0.08
3.4	7.24 ± 0.32	2942 ± 2	9.0 ± 2.0	-0.01 ± 0.10
7	7.28 ± 0.10	2943 ± 1	10.0 ± 1.5	0.04 ± 0.01
12	8.13 ± 0.66	2946 ± 2	9.0 ± 1.0	0.04 ± 0.03
24	7.04 ± 0.19	2945 ± 1	8.5 ± 1.0	0.05 ± 0.02
49	7.39 ± 0.09	2946 ± 1	10.0 ± 0.5	0.04 ± 0.01
74	7.95 ± 0.10	2947 ± 1	10.0 ± 1.0	0.05 ± 0.02
91	6.98 ± 0.10	2948 ± 1	8.5 ± 1.5	0.06 ± 0.02
100	6.13 ± 0.70	2950 ± 1	8.5 ± 1.0	0.09 ± 0.02

and disappear close to 50%. The amplitude of the $\nu_s(CH_3)$ is low at 0.3% acetic acid but then remains almost constant over the whole concentration range, as seen in Figure 7a, where the fitted peak amplitudes are shown. The variations of the fitting parameters for the symmetric methyl stretch as a function of acetic acid concentration are shown in Table 1, where the change of the peak position, which increases in frequency with increasing acid concentration, is noteworthy. This shift can be explained in terms of structural changes at the surface (vide infra). On the other hand, the width of the $\nu_s(CH_3)$ peak as well as the χ_{NR}, are practically constant along the whole concentration range.

If one follows the same procedure as for the C═O stretch in Figure 3b, the symmetric methyl stretch amplitudes have been normalized by the surface number density, resulting in the graph shown in Figure 7b. This figure similarly reveals that the normalized amplitude decreases steeply at low concentrations, but this is followed by a concentration range where the values start to even out, and at concentrations higher than 24%, the normalized amplitude basically remains constant.

Upon increasing concentration, the features in the sps spectrum progressively vanish, and at 49% acetic acid, there are no evident peaks. In the ppp spectrum, the peak at 3620 cm^{-1} decreases at higher concentrations, and after 49%, it disappears completely. The asymmetric methyl stretch at 2970 cm^{-1} is present at concentrations up to 100% acetic acid.

4.3. Theoretical Model and Orientation Analysis. *4.3.1. Orientation of the C═O Group.* There have been relatively few SF studies of the carbonyl group[32−34] compared to the large number of studies performed on the methyl group, and to our knowledge, no formal orientation analysis has been performed on the C═O vibration. The orientation analysis will follow the outline given in the theoretical section. In this work, to a first approximation, the C═O bond is treated as having $C_{\infty v}$ symmetry, which essentially implies that the carbonyl group is considered to be isolated from the rest of the molecule, an assumption supported by ab initio calculations, where ν(C═O) is assigned a value of 89% of the potential energy distribution (PED)[35] (ν_s(CC−O) is assigned a PED value of 8%). Further refinement of this model will be discussed in the following text. There are three nonzero hyperpolarizabilities for the $C_{\infty v}$ point group, as shown in eq 7 and expressed in molecular coordinates (the *c* axis is along the bond, while the *ab* plane is perpendicular to it).

$$\beta_{aac} = \beta_{bbc}\,;\beta_{ccc} \tag{7}$$

All of these hyperpolarizabilities represent symmetric modes[36] (the superscript (2) is not shown for simplicity). To determine the net orientation of this bond, it is necessary to know the relative values between the nonzero $\beta^{(2)}$'s, which can be estimated in this case directly from the Raman depolarization ratio, because there are only two independent hyperpolarizabilities, and those have equal dipole transition moments (μ_c). From eq 1, it follows that

$$r = \beta_{aac}/\beta_{ccc} = \alpha_{aa}/\alpha_{cc} \tag{8}$$

The parameter *r* is related to the Raman depolarization ratio ρ according to eq 9[37]

$$\rho = \frac{3}{4}\left[1 + \frac{5}{4}\left(\frac{2r+1}{r-1}\right)^2\right]^{-1} \tag{9}$$

The value of ρ reported in the literature for the C═O stretch is 0.10,[38,39] which agrees with the ratio obtained in our experiments. Our Raman measurements were performed at 24% acetic acid, which is lower than the value of 30% where linear dimers are first detected.[40] Therefore, our experimental value should correspond to the depolarization ratio of acetic acid hydrated monomers. With a depolarization ratio of 0.10, two values of the parameter *r* satisfy eq 9: 0.3 and 12, of which the latter is regarded as physically unreasonable, because the change in polarizability along the bond direction should be higher rather than perpendicular to it. Hence, $r = 0.3$ is used in the following calculations. The nonzero hyperpolarizabilities (eq 7) are transformed to the laboratory-fixed system as described in the theoretical section. Because the liquid is isotropic in the surface

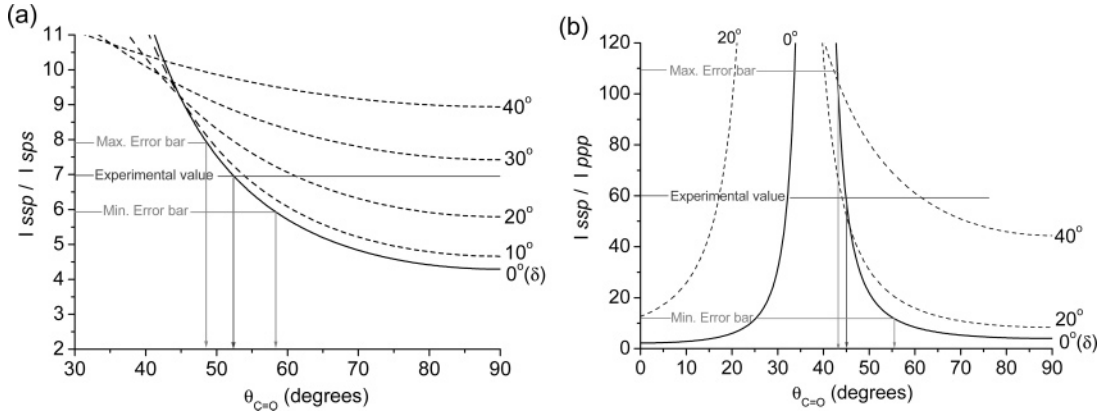

Figure 8. Calculated curves for the relative intensity of the ν(C═O) mode between (a) ssp and sps and (b) ssp and ppp-polarized spectra. The solid curve and dashed curves refer to δ and Gaussian distribution of angles, respectively. $\theta_{C=O}$ is the angle of the C═O bond with respect to the surface normal.

plane, the hyperpolarizabilities are averaged over the azimuthal angles, giving rise to the following expressions for $\chi^{(2)}$

$$\chi_{YYZ} = \frac{N}{\epsilon_0}\langle\beta_{YYZ}\rangle = \frac{1}{2}\frac{N}{\epsilon_0}\beta_{ccc}[(r+1)\langle\cos\theta\rangle + (r-1)\langle\cos^3\theta\rangle] \quad (10a)$$

$$\chi_{YZY} = \frac{N}{\epsilon_0}\langle\beta_{YZY}\rangle = \frac{1}{2}\frac{N}{\epsilon_0}\beta_{ccc}(1-r)(\langle\cos\theta\rangle - \langle\cos^3\theta\rangle) \quad (10b)$$

$$\chi_{ZZZ} = \frac{N}{\epsilon_0}\langle\beta_{ZZZ}\rangle = \frac{N}{\epsilon_0}\beta_{ccc}[r\langle\cos\theta\rangle + (1-r)\langle\cos^3\theta\rangle] \quad (10c)$$

where $\langle\beta_{IJK}\rangle$ denotes averaging over azimuthal angles. The C═O bond does not have a twist angle ϕ because it is assumed to have $C_{\infty v}$ symmetry. The only angle that remains to be determined then is the tilt angle $\theta_{C=O}$ of the C═O bond. $\theta_{C=O}$ is estimated by using the value of the ratio of intensities obtained by different polarization combinations in the theoretical graphs of SF intensity versus $\theta_{C=O}$, which will depend on the assumed distribution function of the molecular tilt angles about the surface normal. In our model, a delta function (δ) was first assumed, and then, a more realistic Gaussian function was employed to describe the distribution of angles (eq 11):

$$\langle f(\theta)\rangle = \frac{1}{\sigma\sqrt{2\pi}}\int_0^\pi f(\theta)\exp\left(-\frac{(\theta-\theta_0)^2}{2\sigma^2}\right)\sin\theta\,d\theta \quad (11)$$

where θ_0 refers to the mean orientation angle, σ^2 to the variance, and $f(\theta)$ to the averaging function (i.e., $\cos\theta$ or $\cos^3\theta$, which are then used in eq 10). In Figure 8, plots of the intensity ratios for the polarization combinations ssp/sps and ssp/ppp are shown. These intensities are dependent on the respective nonlinear susceptibilities and the Fresnel factors. In the calculation of the Fresnel factors, a total of nine refractive indices are required:[12,41] three for each bulk phase ($n_{1(SFG)}$, $n_{1(vis)}$, $n_{1(IR)}$, $n_{2(SFG)}$, $n_{2(vis)}$, and $n_{2(IR)}$, where 1 and 2 refer to the gas-phase and liquid acetic acid solution, respectively) plus three more for the interface ($n'_{(SFG)}$, $n'_{(vis)}$, and $n'_{(IR)}$). The vapor-phase refractive indices were trivially set to 1 ($n_{1(SFG)} = n_{1(vis)} = n_{1(IR)} = 1$), the refractive index of vacuum. The dispersion for the SF and visible beams, being so close in frequency and far away from resonances, was considered to be negligible. As a consequence, the bulk liquid refractive indices were set to $n_{2(SFG)} = n_{2(vis)} = 1.35$.[42] The remaining refractive indices were set to be equal to the bulk visible values. Fortunately, the obtained simulated curves appearto be only weakly dependent on the $n_{2(IR)}$ and n' values assumed. The intensity I in the theoretical curves is proportional to the square of the fitting parameter A obtained from experimental values.

In Figure 8, the solid curves correspond to the simulated intensity ratios when a delta function (δ) is used to describe the distribution of angles, while the dashed curves refer to Gaussian distribution functions for different arbitrary standard deviations (σ), which are presented next to each curve. The mean experimental values are shown as solid horizontal lines, with the corresponding error bars in gray. In the I_{ssp}/I_{sps} plot, the experimental value of a 7% solution was used, which is considered representative of the whole concentration range, as the ratios remain essentially constant (see Figure 4). For a δ distribution, where it is assumed that all molecules have exactly the same orientation, the value of $\theta_{C=O}$ ranges from 48° to 58° (grey arrows), with a mean value of 52° (black arrow). The range in angles is obtained from the dispersion in the experimental data. For the case of Gaussian distribution curves, if only the mean experimental value is considered (solid horizontal line), the I_{ssp}/I_{sps} plot indicates that different $\theta_{C=O}$ are possible depending on the standard deviation chosen. For example, it is observed that for a standard deviation of 10° the mean orientation angle is 54°. Subsequently, 61 ± 20°, and in the extreme case, 90 ± 27°, will also comply with the experimental mean ratio, although the actual intensities in the latter case (I_{ssp} and I_{sps}) will be close to zero and as such should not be considered possible. This implies that the possible distributions of angles are relatively narrow, even though the center angle could range from 52° to an angle close to the surface plane. This range will be further constrained later.

In Figure 8b, the ratio I_{ssp}/I_{ppp} is shown. The large error bars are a consequence of the much lower intensities obtained for the ppp spectra. Fortunately, the theoretical curves are fairly insensitive to the intensity ratio in the experimental range, and useful data can be extracted. For a δ distribution, two values are possible. However, because the results obtained from both polarization combination ratios should be consistent, the cut at lower tilt angles is disregarded. The obtained tilt values in this case range from 43° to 56°, which overlaps the results from I_{ssp}/I_{sps}, an agreement which inspires greater confidence in the theoretical model employed. In the Gaussian distribution curves, the same consistency is observed.

From this analysis, it is concluded that $\theta_{C=O}$ is 52 ± 4° if a δ distribution of angles is assumed. At this point, it is worth mentioning that the polar orientation of the C═O bond (whether

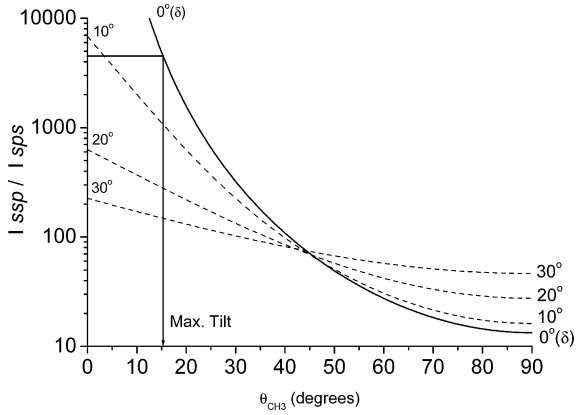

Figure 9. Calculated curves for the relative intensity of the $\nu_s(CH_3)$ mode between ssp and sps-polarized spectra. The solid curve and dashed curves refer to δ and Gaussian distribution of angles, respectively. θ_{CH_3} is the angle of the C_3 axis of the methyl group with respect to the surface normal.

it points toward the bulk liquid or gas phase) cannot be obtained directly from our experimental data, because the phase of the emitted SF light with respect to a known reference was not measured.[43] However, it can be inferred indirectly from the position of the C═O stretching peak in the SF spectra that the carbonyl group is pointing toward the aqueous phase, as discussed in detail in the preceding paper.[26]

4.3.2. Orientation of the Methyl Group. Orientation analysis based on the tilt angle of terminating methyl groups has been commonly employed in sum frequency spectroscopy.[44−47] In the acetic acid molecule, there are three stretching vibrations for the methyl group of the monomer in the gas phase:[30] $\nu_s(CH_3)$, $\nu_a(CH_3)$, and $\nu_{s'}(CH_3)$ at 2944, 2996, and 3051 cm^{-1}, respectively. The large split of more than 50 cm^{-1} between the two asymmetric modes ($\nu_{s'}$ and ν_a) suggests that the true symmetry of the methyl group should be C_s, despite having a low internal rotational barrier[48] (0.88 *kT*). However, to simplify the analysis, C_{3v} symmetry is assumed for the methyl group in the following calculations, which reduces the number of independent hyperpolarizability elements for the symmetric stretch to only two independent components instead of four for C_s symmetry (vide infra). In the SF spectra shown in this report, only the $\nu_s(CH_3)$ and $\nu_a(CH_3)$ were observed. The nonzero components of $\beta^{(2)}$ in the C_{3v} point group for $\nu_s(CH_3)$ are identical to the ones discussed for $C_{\infty v}$ in eq 7: $\beta_{aac} = \beta_{bbc}$; β_{ccc}. On the other hand, for the asymmetric stretches (degenerate in C_{3v}), after averaging over the torsional angles and assuming a symmetric Raman tensor (far away from electronic transitions, $\alpha_{ac} = \alpha_{ca}$), only one independent $\beta^{(2)}$ component remains: $\beta_{aca} = \beta_{caa} = \beta_{bcb} = \beta_{cbb}$.

If one follows the procedure described already for $C_{\infty v}$, the ratio β_{aac}/β_{ccc} can be obtained from the Raman depolarization ratio of the symmetric methyl stretch. The literature value of ρ is 0.02,[49] which is in accordance with our experimental data. From eq 9, the possible values of *r* are 0.6 and 1.9. The latter is used following the arguments of the polarization method of Zhang et al.[50] Subsequent transformation of the hyperpolarizabilities to the laboratory frame coordinates leads to the same set of equations as for $C_{\infty v}$ (eq 10). In Figure 9, a plot of the intensity ratios of the polarization combinations ssp/sps is shown, where a δ and Gaussian function distribution were considered for the tilt angle (θ_{CH_3}). In the calculation of the theoretical curve shown in Figure 8, the same refractive indices as those proposed for C═O were used. These assumptions are justified by the fact that θ_{CH_3} is not very sensitive to changes in $n_{2(IR)}$ or n'.

Although $\nu_s(CH_3)$ was not seen for the sps polarization combination, the noise level allowed an upper limit to the strength of this mode to be set ($A_{sps}\ \nu_s(CH_3) < 0.10$ au), constraining the experimental I_{ssp}/I_{sps} ratio to be greater than 4600. This lower limit in the ratio remains essentially constant along the whole concentration range. The confidence in the calculated noise level for the sps polarization combination was strengthened after analyzing the spectra of acetic acid in D_2O (spectra not shown), where the hydrogen-bonded OH stretch of the acid is absent, allowing an unambiguous deconvolution of the spectral features.

In Figure 9, the maximum possible tilt angle is seen to be close to 15° when a δ distribution of angles is assumed. For the Gaussian functions, the highest possible angular distribution is $\sigma = 11°$ for a center angle of $\theta_o = 0°$, which represents an even lower distribution of angles than that obtained for $\theta_{C=O}$.

A second estimate of the methyl tilt angle can be obtained from studying the asymmetric methyl stretch, which was clear in the ppp spectra. In this case, the nonzero $\chi^{(2)}$ tensor elements can be written exclusively as functions of the hyperpolarizability element β_{aca}, as shown in eq 12. All intensity ratios are therefore independent of the actual $\beta^{(2)}$ element values. As no clear peak was observed for the ssp polarization combination, the noise level in this spectrum was used to obtain the maximum experimental I_{ssp}/I_{ppp} ratio. The tilt angle of the methyl group determined through this procedure was constrained to be lower than 20° for a δ distribution of angles (theoretical curve not shown), a result which increases the confidence of our theoretical model for the methyl group.

$$\chi_{YYZ,d} = \frac{N}{\epsilon_0}\langle\beta_{YYZ,d}\rangle = -\frac{N}{\epsilon_0}\beta_{aca}\sin^2\theta\cos\theta \qquad (12a)$$

$$\chi_{YZY,d} = \frac{N}{\epsilon_0}\langle\beta_{YZY,d}\rangle = \frac{N}{\epsilon_0}\beta_{aca}\cos^3\theta \qquad (12b)$$

$$\chi_{ZZZ,d} = \frac{N}{\epsilon_0}\langle\beta_{ZZZ,d}\rangle = 2\frac{N}{\epsilon_0}\beta_{aca}\sin^2\theta\cos\theta \qquad (12c)$$

A third estimate of θ_{CH_3} could have been obtained comparing the amplitudes of $\nu_s(CH_3)$ observed in the ssp spectra with $\nu_a(CH_3)$ detected in the ppp spectra. The advantage of this latter case is that there is no need to rely on the noise level to calculate the experimental ratio because clear peaks were observed in both polarizations. Unfortunately, the relative values of the hyperpolarizabilities β_{aac} and β_{aca} of acetic acid, required in the calculation of the theoretical curve, were unknown. As a consequence, this supplementary analysis could not be performed.

From the analysis of the methyl and carbonyl groups, the average orientation of the acetic acid molecule at the surface can be established. The two tilt angles calculated in this report ($\theta_{C=O}$ and θ_{CH_3}) and shown in sketches in Figure 10 allow the possible orientations at the surface to be constrained to a rather narrow window. For this purpose, knowledge of the actual geometrical angles between the different atoms in the molecule is necessary. The equilibrium structural parameters of acetic acid have been reported earlier,[39,51] where the angles −(C−C═O) and −(C−C−O) were found to be 126° and 112°, respectively.

By taking these angles and the arguments in the preceding paragraphs into account, the following conclusions can be

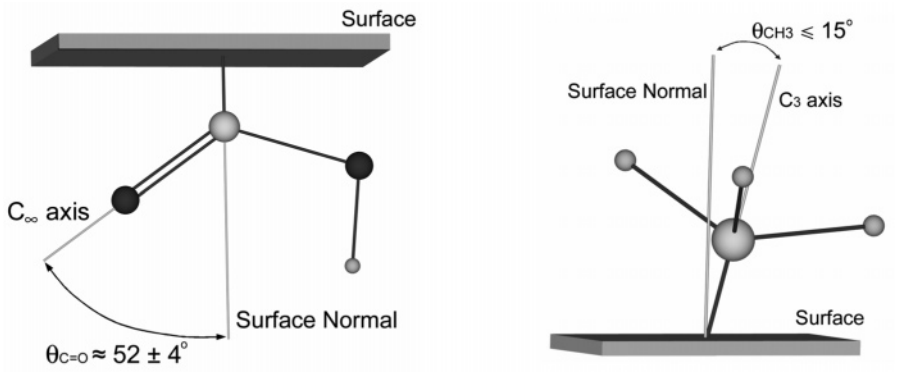

Figure 10. Sketches of the carbonyl (a) and methyl (b) orientations with respect to the surface normal. The angles shown were calculated under the assumption of a δ distribution of angles.

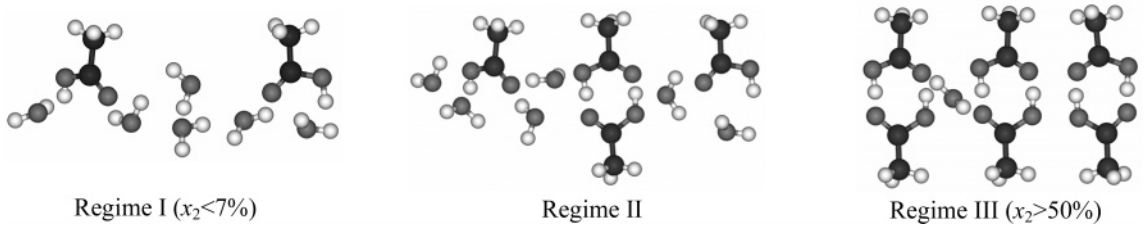

Figure 11. Sketch of the proposed surface structure at different concentrations. Black, gray, and white spheres represent carbon, oxygen, and hydrogen atoms, respectively.

drawn: The acetic acid molecules remain at a constant orientation with a narrow distribution of angles, with their methyl groups protruding out into the gas phase and aligned close to the surface normal (maximum tilt of $0 \pm 11°$ from the surface normal). Because the C_3 axis is essentially perpendicular to the surface plane, the possible tilt angles of the C═O bond from the surface normal, exclusively on the basis of θ_{CH_3}, can be reduced to a fairly narrow range extending from 44° to 65°. Fundamentally, the same range was independently calculated from the SF spectra of the carbonyl group showing great consistency, so it can be stated with a certain confidence that the C═O bond is directed toward the liquid phase with an angle of $55 \pm 11°$ from the surface normal when assuming a Gaussian distribution of angles, in the concentration range where it was detected. Finally, the tilt angle of the C—O bond can be inferred from the C═O and CH_3 angles to be fairly close to the surface plane ($\theta_{C-O} \approx 70°$), which explains in large part the weakness of the C—O stretching mode in the ssp spectra shown in the preceding paper of this issue.

4.3.3. Orientation Analysis of Water. The orientation of interfacial water molecules in pure water and in 0.3% acetic acid has been determined as a reference for the orientation analysis of acetic acid molecules. In the analysis of pure water, only the ssp and ppp spectra were used, because the signal-to-noise ratio in the sps spectrum is low and lacks distinct peaks (Figure 5). The free OH bond is assumed to have $C_{\infty v}$ symmetry like the C═O group of acetic acid and is therefore treated similarly in the orientation analysis. According to eq 7, the three nonvanishing hyperpolarizabilities, $\beta_{aac} = \beta_{bbc}$ and β_{ccc}, can be related to each other using the Raman depolarization ratio ρ, from which the parameter $r = \beta_{aac}/\beta_{ccc} = \alpha_{aa}/\alpha_{cc}$ can be determined, as discussed already. A value of $r = 0.32$ is reported in the literature.[52] The refractive indices used in the calculations are $n_{2(SFG)} = n_{2(vis)} = 1.34$, $n_{2(IR)} = 1.18$ (3700 cm^{-1}), $n'_{SFG} = n'_{vis} = 1.14$, and $n'_{IR} = 1.10$.[28] If one assumes a δ distribution of the tilt angle of the free OH bond (θ_{OH}), an isotropic azimuthal distribution, and follows the same procedure as for the C═O group, the result of $34° < \theta_{OH} < 36°$ is obtained. This is to be compared to previous estimates $\theta_{OH} \leq 38°$,[13] and $\theta_M = 51°$ [28] in a step functional distribution, where $0 < \theta_{OH} < \theta_M$. In the last case, the fast orientation motion of the molecules was considered in the analysis. Thus, the tilt angle θ_{OH} obtained in these experiments agrees with other values reported in the literature.

The same analysis was performed for 0.3% acetic acid, as clear peaks for the free OH bond were detected (Figure 5). The tilt angle θ_{OH} at this concentration is higher: $37° < \theta_{OH} < 39°$. However, despite increased scatter in the experimental data, a narrow range of angles is obtained also. This is a consequence of the shape of the theoretical curve (not shown), which becomes more insensitive at higher I_{ssp}/I_{ppp} ratios. On the other hand, if a Gaussian function is used instead of the mathematically convenient Dirac's δ function to describe the distribution of angles, the difference between pure water and 0.3% acid is no longer significant, as it can be accounted for by a slight difference in the standard deviation, which is higher for the 0.3% case. These results indicate that upon the addition of small amounts of acetic acid, patches of unperturbed water can still be found at the surface. However, on the basis of the amplitude obtained from the fitting of the free OH peak, the decrease in the number of water molecules contributing to the sum frequency signal is approximately 40%, while the surface concentration has only decreased by less than 10% ($x_2^s = 8\%$), which implies a strong perturbation of the overall water surface structure.

4.4. Describing the Surface of Acetic Acid Aqueous Solutions. On the basis of the results discussed here and in the preceding paper,[26] the surface of aqueous acetic acid solutions can be conveniently divided into three main concentration regimes to describe the structuring at the surface. A sketch of the proposed surface structure of the aqueous acetic acid solutions at different concentration regimes is shown in Figure 11.

Regime I (x_2 < 7%/x_2^s < 55%). In the pure water surface, a fraction of the molecules have an OH bond protruding into the gas phase with an average tilt angle (θ_{OH}) close to 35° from

the surface normal. The remaining molecules have their OH bonds forming hydrogen bonds of varying strengths with the other surface neighbors. Upon addition of tiny amounts (x_2 = 0.3%) of acetic acid, the surface water structure is considerably perturbed: The amplitudes of the main features observed in the pure water spectrum are reduced by more than 40%, while clear peaks belonging to the acid, like the symmetric methyl stretch (2943 cm^{-1}), carbonyl stretch (1720 cm^{-1}), and hydrogen-bonded hydroxyl stretch (~2975 cm^{-1}), make its presence at the surface obvious. This perturbation is expected, because the acid tends to preferentially adsorb at the surface, as observed in surface tension measurements. The actual surface concentration of acetic acid differs appreciably from the bulk, especially at low concentrations where for x_2 = 0.3% the surface concentration was estimated to be as high as x_2^s = 8%. It is interesting to observe that less than 10% of acetic acid at the surface is enough to extensively disrupt the water structure, as evidenced by the reduced amplitudes of the peaks recognized from the pure water surface. Moreover, the presence of the acetate anion at the surface can be excluded, because no evidence of the carboxylate stretching vibrations were observed. This finding is not unreasonable, as charged species will tend to be depleted at the surface, particularly when the hydrophobic driving force to the surface is only a single methyl group.

At a bulk concentration of x_2 = 1.6% (spectra not shown), which corresponds at the surface to $x_2^s \approx$ 30%, all features from the pure water spectrum have completely disappeared. The only signs of surface water with a preferred orientation are from very weakly or non-hydrogen-bonded molecules (~3620 cm^{-1}), which are not present in pure water and are therefore related to specific interactions with the acetic acid. On the other hand, the characteristic vibrations of the acid increase in intensity, but no new peaks are observed. The single peak observed in the C═O stretching range is attributed to the hydrated monomer (M_h) species of the acetic acid, which is believed to be the only species present at the surface in this regime.

Regime II (Interfacial Bilayer Formation). When increasing the concentration to x_2 = 7% ($x_2^s \approx$ 55%), a maximum in the amplitude of the C═O vibration is observed (Figure 3a), after which it slowly decreases, disappearing at concentrations slightly higher than x_2 = 43% ($x_2^s \approx$ 77%), despite the ever-rising surface concentration of acid. This is explained by the formation of the centrosymmetric cyclic dimer in detriment to the hydrated monomer (M_h), which gives rise to the C═O stretching peak seen in the SF spectra at 1720 cm^{-1}, as discussed in the preceding paper. This picture is supported by the orientation analysis performed in a previous section, where it was found that the acetic acid M_h remains in a constant orientation with a narrow distribution of angles, in the whole concentration range where it is present. The cyclic dimer, with its sum frequency inactive C═O stretch, is thought to first appear at the surface at concentrations lower than x_2 = 7%, increasing rapidly in numbers and taking over the whole surface at approximately x_2 = 50%, which corresponds to a surface concentration of $x_2^s \approx$ 80%. Furthermore, the two other vibrations related to the hydrated monomer at ~2975 cm^{-1} (hydrogen-bonded hydroxyl stretch) and ~3620 cm^{-1} (weakly or non-hydrogen-bonded water) follow the same tendency as the C═O band.

The fact that the methyl stretching vibration is detected over the entire concentration range (Figure 7a) also strengthens the cyclic dimer argument, as it confirms the constant orientation of the methyl group, even after the disappearance of the C═O vibration when the dimer is dominant at the surface. Moreover, the noncancellation of the methyl signal when the cyclic dimer is dominant is explained in terms of the different environments (vapor and condensed bulk phase) in which the two opposing methyl groups vibrate.[26] However, the decrease and subsequent leveling off in the normalized $\nu_s(CH_3)$ amplitudes (Figure 7b) is attributed to partial cancellation associated with the formation of the dimer.

The lack of signal for the C═O band at higher concentrations could also be interpreted in terms of an increased disorder. However, the data gathered from the different vibrational modes, like the constant tilt orientation of the methyl group (θ_{CH_3}), allow this option to be discarded in favor of the opposite argument: an extended organization of the surface layer with the formation of the cyclic dimer. The driving force for the cyclic dimer to preferentially adsorb at the surface where its conformational freedom will be unavoidably restrained can be explained by its zero dipole moment, which will cancel the charge-mirroring effect[53] that other acetic acid species having a net dipole moment would experience, like, for example, the linear dimer. The charge-mirroring effect results from the van der Waals force that a charge or dipole would experience near a surface due to reflection of the field from the same surface. This force will be repulsive in this particular case, because the dipole is approaching the surface from the condensed phase.

At this point, it is worth mentioning that the surface concentration of acetic acid, which was calculated using the monolayer model (Section 4.1), becomes less sound in this regime, as the formation of a cyclic dimer is not accounted for in that approximation. As a consequence, the reported x_2^s in Regimes II and III should be considered as rough estimates. More elaborate models will be discussed in detail in a forthcoming publication.

Regime III (x_2 > 50%/x_2^s > 80%). From x_2 = 50% up to pure acid, no major changes are observed on the surface (surface concentration increases slightly from $x_2^s \approx$ 80% to 100%). However, at the pure acetic acid surface, a small decrease in the normalized $\nu_s(CH_3)$ amplitude, as well as a step feature observed in the C═O stretching region (shown in preceding paper) where the constructive interference is now seen at low wavenumbers, and slight blue shift of the $\nu_s(CH_3)$ peak position, could be evidence of a small structuring change.

5. Conclusions

A thorough study of the surface of aqueous acetic acid solutions has been performed using vibrational sum frequency spectroscopy in conjunction with surface tension measurements. The stretching vibrations of the C═O and CH_3 groups of acetic acid, as well as the OH bonds of water, were targeted under different polarization combinations to obtain a comprehensive picture of the surface behavior, including the orientation of specific bonds. The fact that two different bonds of acetic acid were investigated allowed a narrowing of the uncertainty in the orientational determination, and through internal consistency checks, greater confidence in the theoretical model used in the analysis was achieved. The acetic acid molecule was found to remain in a basically upright position throughout the concentration range, extensively disturbing the water surface structure from the very first addition at 0.3%. The dominant acetic acid species at low bulk concentration is the hydrated monomer (M_h), whereas the presence of the cyclic dimer species was inferred from the data, first appearing at concentrations slightly lower than 7% and saturating the surface close to 50% bulk acid concentration.

Acknowledgment. Financial support from the Swedish Research Council (VR), the Swedish Research Council for Engineering Sciences (TFR), and the Swedish Foundation for Strategic Research (SSF) are gratefully acknowledged. We thank Dr. Colin Bain (Oxford University, U.K.), Prof. Em. Jan Christer Eriksson and Prof. Per Claesson (KTH, Sweden) for valuable and inspiring discussions. We also thank Prof. Gabor Somorjai (UC Berkeley, U.S.A.) for encouragement and guidance while building up our VSFS facility. We thank Prof. Lars Kloo and Martin Lindsjö at Inorganic Chemistry KTH for making their BioRad Raman spectrometer available to our studies.

7. Appendix

Refinement in the Orientation Analysis of the C═O Bond. This discussion was based on the approximation of the carbonyl group being isolated from the rest of the molecule ($C_{\infty v}$ symmetry). However, a more realistic treatment would be to consider the C═O bond as C_s symmetry, in which case the number of independent hyperpolarizabilities for the symmetric stretching vibration increases to four (β_{aac}, β_{bbc}, β_{ccc}, $\beta_{cac} = \beta_{acc}$). The relative values of the different hyperpolarizabilities could be obtained from the Raman tensor elements, but these are rarely known. Nonetheless, it seems reasonable to assume than the off-diagonal elements of the Raman tensor are much lower than the diagonal ones,[46] which will reduce the number of independent β's to three. In contrast to $C_{\infty v}$, $\beta_{aac} \neq \beta_{bbc}$ for C_s symmetry, and therefore, the two Raman polarizability elements perpendicular to the bond direction are distinguishable. In what follows, the coordinate axis *c* is considered as before along the C═O bond, *a* at right angles in the plane of the carboxyl group (COOH), and *b* perpendicular to the *ac* plane.

In this case, the depolarization ratio (ρ) is not sufficient to determine the actual ratios between the different hyperpolarizabilities, as there are three unknown tensor elements: α_{aa}, α_{bb}, and α_{cc}. However, if the relative value between two different elements is assumed, then eq A1[37] allows the third element to be calculated from ρ. After the transformation of the hyperpolarizabilities from the molecular (*abc*) to the laboratory fixed (*XYZ*) system, a random distribution for the azimuthal angle ($\chi_{C=O}$) can be reasonably assumed. Nevertheless, the same assumption will unquestionably be invalid for the twist angle ($\phi_{C=O}$), because it is directly linked to the tilt angle of the methyl group (θ_{CH_3}), which was proved already to have a preferred tilt at the surface. Simulations were performed (theoretical curve not shown) for a set of different relative Raman tensor elements, bearing in mind that the polarizability derivative in the bond direction (α_{cc}) is expected to be highest, followed by the Raman element in the carboxylic plane (α_{aa}). Moreover, a δ distribution of twist angles of 0° and 15° were used, corresponding to the minimum and maximum θ_{CH_3}.

$$\rho = \frac{3(\gamma')^2}{45(a')^2 + 4(\gamma')^2} \quad \text{(A1a)}$$

$$a' = \frac{1}{3}(\alpha_{aa} + \alpha_{bb} + \alpha_{cc}) \quad \text{(A1b)}$$

$$\gamma'^2 = \frac{1}{2}[(\alpha_{aa} - \alpha_{bb})^2 + (\alpha_{bb} - \alpha_{cc})^2 + (\alpha_{cc} - \alpha_{aa})^2] \quad \text{(A1c)}$$

The results obtained from this routine when compared with the experimental values show that the $\theta_{C=O}$ changes only slightly in a wide range of possible α_{aa}/α_{cc} values, diverging only for values very close to 1 where it is no longer physically reasonable. For values of $\alpha_{aa}/\alpha_{cc} > 1$, the experimental value did not cut the calculated curve. It can be concluded that the initial assumption where the $C_{\infty v}$ point group was employed, where implicitly it was assumed that $\alpha_{aa} = \alpha_{bb}$, was a good approximation, and for this particular case, similar results are obtained when assuming a C_s symmetry.

References and Notes

(1) Maréchal, Y. *J. Chem. Phys.* **1987**, *87*, 6344.
(2) Bratož, S.; Hadži, D.; Sheppard, N. *Spectrochim. Acta* **1956**, *8*, 249.
(3) Semmler, J.; Irish, D. E. *J. Solution Chem.* **1988**, *17*, 805.
(4) Bertie, J. E.; Michaelian, K. H. *J. Chem. Phys.* **1982**, *77*, 5267.
(5) Nakabayashi, T.; Kosugi, K.; Nishi, N. *J. Phys. Chem. A* **1999**, *103*, 8595.
(6) Nakabayashi, T.; Nishi, N. *J. Phys. Chem. A* **2002**, *106*, 3491.
(7) Kosugi, K.; Nakabayashi, T.; Nishi, N. *Chem. Phys. Lett.* **1998**, *291*, 253.
(8) Adamson, A. W.; Gast, A. P. *Physical Chemistry of Surfaces*, 6th ed.; Wiley-Interscience: New York, 1997.
(9) Hirose, C.; Yamamoto, H.; Akamatsu, N.; Domen, K. *J. Phys. Chem.* **1993**, *97*, 10064.
(10) Hirose, C.; Akamatsu, N.; Domen, K. *Appl. Spectrosc.* **1992**, *46*, 1051.
(11) Hirose, C.; Akamatsu, N.; Domen, K. *J. Chem. Phys.* **1992**, *96*, 997.
(12) Zhuang, X.; Miranda, P. B.; Kim, D.; Shen, Y. R. *Phys. Rev. B* **1999**, *59*(19), 12632.
(13) Du, Q.; Superfine, R.; Freysz, E.; Shen, Y. R. *Phys. Rev. Lett.* **1993**, *70*, 2313.
(14) Zhang, D.; Gutow, J. H.; Eisenthal, K. B.; Heinz, T. F. *J. Chem. Phys.* **1993**, *98*, 5099.
(15) Shultz, M. J.; Schnitzer, C.; Simonelli, D.; Baldelli, S. *Int. Rev. Phys. Chem.* **2000**, *19*, 123.
(16) Bloembergen, N.; Pershan, P. S. *Phys. Rev.* **1962**, *128*, 606.
(17) Shen, Y. R. *The principles of Nonlinear Optics*, 1st ed.; John Wiley & Sons: New York, 1984.
(18) Colles, M. J.; Griffiths, J. E. *J. Chem. Phys.* **1972**, *56*, 3384.
(19) Smith, J. M.; Van Ness, H. C. *Introduction to Chemical Engineering*, 4th ed.; McGraw-Hill: New York, 1987; pp 379−380, 409−413.
(20) Sebastiani, E.; Lacquaniti, L. *Chem. Eng. Sci.* **1967**, *22*, 1155.
(21) Rubio, R. G.; Diez-Pascual, A.; Coto, B.; Crespo-Colin, A.; Compostizo, A. *Phys. Chem. Chem. Phys.* **2003**, *5*, 4864.
(22) Guggenheim, E. A.; Adam, N. K. *Proc. R. Soc. A* **1933**, *139*, 218.
(23) Kipling, J. *J. Colloid Sci.* **1963**, *18*, 502.
(24) Eriksson, J. C. *Ark. Kemi* **1966**, *26*, 49.
(25) Berg, J.; Claesson, P. *Thin Solid Films* **1989**, *178*, 261.
(26) Johnson, C. M.; Tyrode, E.; Baldelli, S.; Rutland, M. W.; Leygraf, C. *J.* Phys. Chem. A **2004**, preceding article in this issue.
(27) Superfine, R.; Guyot-Sionnest, P.; Hunt, J. H.; Kao, C. T.; Shen, Y. R. *Surf. Sci.* **1988**, *200*, L445.
(28) Wei, X.; Shen, Y. R. *Phys. Rev. Lett.* **2001**, *86*, 4799.
(29) Liu, D.; Ma, G.; Levering, L.; Allen, H. *J.* Phys. Chem. B **2004**, *108*, 2252.
(30) Haurie, M.; Novak, A. J. Chim. Phys. 1965, *62*, 137.
(31) Haurie, M.; Novak, A. *J. Chim. Phys.* **1965**, 62, 146.
(32) Miranda, P. B.; Du, Q.; Shen, Y. R. *Chem. Phys. Lett.* **1998**, *286*, 1.
(33) Hirose, C.; Bandara, A.; Katano, S.; Kubota, J.; Wada, A.; Domen, K. *Appl. Phys. B.* **1999**, *68*, 559.
(34) Miyamae, T.; Yamada, Y.; Uyama, H.; Nozoye, H. *Appl. Surf. Sci.* **2001**, *180*, 126.
(35) Burneau, A.; Génin, F.; Quilès, F. *Phys. Chem Chem. Phys.* **2000**, *2*, 5020.
(36) Yamamoto, H.; Akamatsu, N.; Wada, A.; Domen, K.; Hirose, C. *J. Electron Spectrosc. Relat. Phenom.* **1993**, 64/65, 507.
(37) Long, D. A. *Raman Spectroscopy*, 1st ed.; McGraw-Hill: London, 1977.
(38) Yokoyama, I.; Miwa, Y.; Machida, K. *J. Phys. Chem.* **1991**, *95*, 9740.
(39) Yokoyama, I.; Miwa, Y.; Machida, K. *Bull. Chem. Soc. Jpn.* **1992**, *65*, 746.
(40) Génin, F.; Quilès, F.; Burneau, A. *Phys. Chem. Chem. Phys.* **2001**, *3*, 932.
(41) Lu, R.; Gan, W.; Wu, B.; Chen, H.; Wang, H. *J. Phys. Chem. B* **2004**, *108*, 7297.
(42) Sims, R. W.; Willcott, M. R.; Inners, R. R. *J. Chem. Phys.* **1979**, *70*, 4562.
(43) Wei, X.; Miranda, P. B.; Zhang, C.; Shen, Y. R. *Phys. Rev. B* **2002**, *66*, 85401

(44) Bell, G. R.; Bain, C. D.; Ward, R. N. *J. Chem. Soc., Faraday Trans.* **1996**, *92*, 515.
(45) Zhung, X.; Miranda, P. B.; Kim, D.; Shen, Y. R. *Phys. Rev. B* **1999**, *59*, 12632.
(46) Bell, G. R.; Li, Z. X.; Bain, C. D.; Fischer, P.; Duffy, D. C. *J. Phys. Chem. B* **1998**, *102*, 94361.
(47) Ye, S.; Morita, S.; Li, G.; Noda, H.; Tanaka, M.; Uosaki, K.; Osawa, M. *Macromolecules* **2003**, *36*, 5694.
(48) Tabor, W. J. *J. Chem. Phys.* **1957**, *27*, 974.
(49) Edall, J. T.; Wilson, E. B. *J. Chem. Phys.* **1938**, *6*, 124.
(50) Zhang, D.; Gutow, J.; Eisenthal, K. B. *J. Phys. Chem.* **1994**, *98*, 13729.
(51) Van Eijck, B. P.; van Opheusden, J.; van Schaik, M. M.; van Zoeren, E. *J. Mol. Spectrosc.* **1981**, *86*, 465.
(52) Murphy, W. F. *Mol. Phys.* **1978**, *36*, 727.
(53) Israelachvili, J. *Intermolecular & Surface Forces*, 2nd ed.; Academic Press: London, 1992.